Report for CERN Summer Student Programme

Indirect constraints on Charm-Yukawa coupling with the ATLAS detector at the LHC

Qassem Awayies

Supervisors: Petar Bokan & Valentina Cairo

July 1st–August 23rd, 2024

Espl. des Particules 1/1211, 23 Genève

Acknowledgement

I would like to thank the following people who have helped me undertake this internship:
My academic advisors, Ahmed Bassalat, and Hadil Aboalrob, for recommending me to this programme;
My supervisors, Petar Bokan, and Valentina Cairo, for their support and patience;
CERN and the Summer Student Programme responsibles and organizers, for such a spectacular opportunity;
Last but not least, my friends and colleagues during this programme, it will take a lot of space to include all of you which my heart already contains.

Contents

Résumé

Depuis la découverte du boson de Higgs par les collaborations ATLAS et CMS au LHC, la question de savoir comment le boson de Higgs interagit avec d'autres particules du modèle standard a été étudiée. On sait que la force du couplage de Higgs est proportionnelle à la masse de la particule à laquelle il se couple. Cependant, le quark Charm, en raison de sa masse relativement faible et de la difficulté de sa détection et de son identification, a du mal à déterminer la force du couplage avec le boson de Higgs. Dans ce travail, les mesures ATLAS $H \to \gamma\gamma$ ont été utilisées pour étudier la production du boson de Higgs induite par le charme afin d'établir des contraintes indirectes sur les valeurs de la force de couplage du quark Charm avec le boson de Higgs, ou ce que l'on appelle le couplage Charm-Yukawa.

Abstract

Since the discovery of the Higgs boson by the ATLAS and CMS collaborations at the LHC, the question of how the Higgs boson interacts with other Standard Model particles has been investigated. It is known that that the Higgs coupling strength is proportional to the mass of the particle it couples to. The Charm quark, however, due to its relatively low mass and difficulty of detection and identification, possesses difficulty in determining the coupling strength with the Higgs boson. In this work, ATLAS $H \to \gamma\gamma$ measurements were used to investigate the Charm induced production of the Higgs boson in order to set indirect constraints on the coupling strength values of the Charm quark with the Higgs boson, or the so called Charm-Yukawa coupling.

1 Introduction

The discovery of Higgs boson by the ATLAS and CMS collaborations [5, 9] in the past decade has risen the question of whether the observed Higgs boson interacts with the rest of the Standard Model (SM) particles as predicted or not. The Large Hadron Colider (LHC) is the world largest particle collider. Located at CERN with a circumference of 26.6 Km, it can accelerate protons up to a center of mass energy of 13.6 TeV.

The ATLAS experiment at the LHC is a multi-purpose experiment designed to study interactions predicted by the SM and search for new phenomena. ATLAS detector consists of: A toroidal magnets system, which is responsible for bending the particle's trajectories in the different detector layers; A muon detector, which is responsible for identifying and measuring the momenta of muons; A calorimeter, which measures the energy the particle loses as it passes through the detector; And the inner detector, which is the very first part of the detectors that observes collision products. Figure 1 shows the different parts of the ATLAS detector.

The coordinates in the detectors are defined such that the z-axis is the beam axis, the x-axis points towards the LHC, and the y-axis points upward. The transverse plane is defined as the xy-plane of the detector. The transverse plane is of special interest because momentum and energy conservation laws can be applied there. The conservation laws cannot be applied in general because protons are composite particles and the initial energies of their constituents that interact in LHC collisions are unknown. The transverse momentum (p_T) of particles is invariant under Lorentz boosts along the beam axis, making it easier to study the momenta of produced particles regardless of the frame of reference.

Direct analysis for measuring the coupling strength between the Charm quark and the Higgs boson do not yield satisfactory results; Higgs boson coupling strength is proportional to the mass of the particle and hence for the quite lighter Charm quark it does not couple as strongly to the Higgs boson as does, for instance, the Top quark. In addition, the decay channel of Higgs boson to a Charm anti-Charm pairs possesses a large background, in addition to the difficulty of identifying Charm induced jets. Nonetheless, ATLAS $H \to c\bar{c}$ analysis [2] sets a limit on the coupling strength to be $y_c < |4.2 \times y_c^{SM}|$.

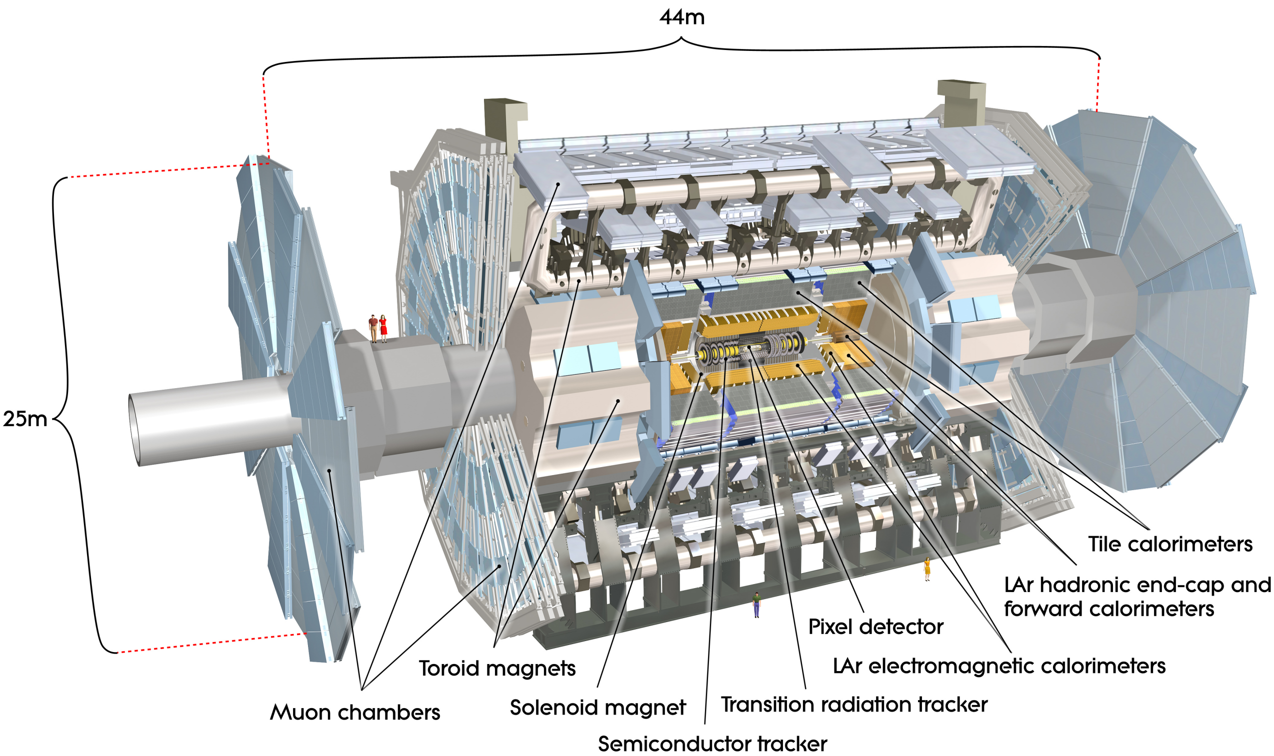

Figure 1: A schematic diagram showing the different parts of the ATLAS detector[6].

1.1 The Higgs boson production modes

An indirect way to study the interaction between the Higgs boson and the Charm quark is by studying Higgs boson produciton. Figure 2 shows the processes that the Higgs boson can be produced by in the LHC. The majority of the Higgs particles at the LHC are produced by the means of gluon-gluon fusion processes (ggF). This process consists of the fusion of two massless gluons to form an intermediate massive fermion loop, which may include the Charm quark, then yielding the Higgs boson. Another way the Higgs boson can interact with the Charm quark during the production process is when a Charm and anti-Charm pair merge together to yield a Higgs boson ($c\bar{c} \to H$). Higgs boson production is described by the total cross-section, which is composed of the individual production modes, that is,

$$\sigma_{pp\to H} = \sigma_{ggF} + \sigma_{t\bar{t}H} + \sigma_{b\bar{b}H} + \sigma_{c\bar{c}H} + \sigma_{VBF} + \sigma_{ZH} + \sigma_{W^-H} + \sigma_{W^+H}. \tag{1}$$

In Equation (1) $x\bar{x}H$ stands for Higgs production from particle x, VBF stands for Vector Boson Fusion processes, while W$^{\pm}$H, and ZH stand for processes where the Higgs boson was produced in association with a W or Z boson. The cross section is proportional to the modulus squared of the amplitude, which is represented by the Feynmen diagrams in Figure 2. However, interference terms contain the product of two different amplitudes, that is, it will depend on the product of two couplings and their relative sign will play a role.

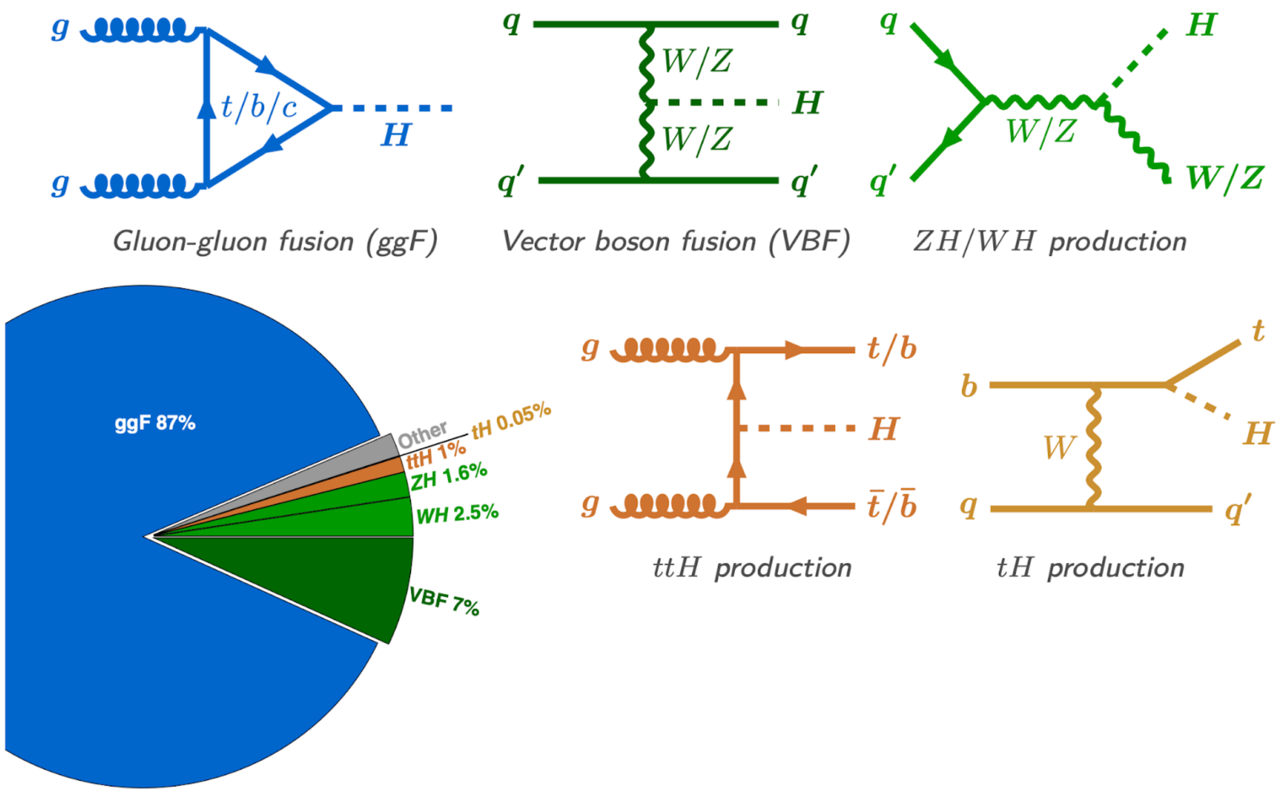

Figure 2: Different production modes of the Higgs boson at the LHC.

2 Charm-Yukawa coupling and the $\kappa-$framework

The interaction between any Standard Model particle and the Higgs boson is expressed in terms of Yukawa coupling strength y_p. To account for any deviations in the Standard Model values of this coupling strength in the measurement, a parametrization framework has been developed. The so-called $\kappa-$framework, parameterizes the cross section with the quantity $\kappa_p = y_p/y_p^{SM}$; where y_p is the observed value of the coupling strength and y_p^{SM} is the Standard Model value of coupling strength. κ_p's are called the coupling modifiers and they are the parameters of interest (POI) in our analysis. Introducing this parametrization to Equation (1) yields,

$$\sigma_{pp\to H}(\kappa,\theta) = \kappa_t^2(\sigma^{t\bar{t}}_{ggF}+\sigma_{t\bar{t}H}+\kappa_t\kappa_b\sigma^{bt}_{ggF}+\kappa_b^2(\sigma^{b\bar{b}}_{ggF}+\sigma_{b\bar{b}H})+\kappa_b\kappa_c\sigma^{bc}_{ggF}+\kappa_c\kappa_t\sigma^{tc}_{ggF}+\kappa_c^2(\sigma^{c\bar{c}}_{ggF}+\sigma_{c\bar{c}H})+\sigma_{\mathrm{other}}. \tag{2}$$

In Equation (2) Charm induced production cross sections scale with κ_c^2, while cross sections that account for interference between different flavours scale linearly with κ_c. In this analysis the value of κ_t was always fixed to unity (the Standard Model value), while two models were considered in terms of κ_b, a model in which $\kappa_b = 1$ (SM) and a model in which κ_b is a free parameter. In addition to parameterizing the cross section, the branching ratio to $H \to \gamma\gamma$ is also parameterised.

The branching ratio is defined as the squared ratio between the decay width (Γ) of the photon and the total decay width of the Higgs boson. The parametrization can be introduced as follows,

$$B = \frac{\kappa_\gamma^2}{\kappa_H^2} \times \left(\frac{\Gamma_\gamma^{SM}}{\Gamma_H^{SM}}\right)^2, \tag{3}$$

with,

$$\kappa_H^2 = 1 - B_{cc} - B_{bb} + \kappa_c^2 B_{cc} + \kappa_b^2 B_{bb} + \kappa_g^2(\kappa_b, \kappa_c) B_{gg} + \kappa_\gamma^2(\kappa_b, \kappa_c) B_{\gamma\gamma} + \kappa_{\gamma Z}^2(\kappa_b, \kappa_c) B_{\gamma Z},$$

$$\kappa_\gamma^2 = 0.99 + 0.0039\kappa_c + 0.0073\kappa_b + 1.5 \times 10^{-5}\kappa_c\kappa_b + 2.9 \times 10^{-6}\kappa_c^2 + 2.1 \times 10^{-5}\kappa_b^2,$$

$$\kappa_{Z\gamma}^2 = 1.00 + 7.8 \times 10^{-4}\kappa_c + 0.0034\kappa_c + 8.7 \times 10^{-7}\kappa_b\kappa_c + 6.1 \times 10^{-8}\kappa_c^2 + 3.2 \times 10^{-6}\kappa_b^2,$$

$$\kappa_g^2 = 1.14 - 0.029\kappa_c - 0.13\kappa_b + 0.0039\kappa_c\kappa_b + 0.00031\kappa_c^2 + 0.012\kappa_b^2,$$

where B_{xx} is the branching ratio of the Higgs boson decaying to particle x.

3 Statistical Procedure

To quantitatively set constraints on the values of the coupling modifiers in Equation (2), the parameterized cross section is fitted to ATLAS data by means of a maximum likelihood fit. For this analysis, ATLAS $H \to \gamma\gamma$ measurements ($\sqrt{s} = 13$ TeV, $\mathcal{L}_{\text{int}} = 139$ fb^{-1}) of the differential cross section were used; it is the final state with the cleanest signal regardless of its low branching ratio. The likelihood function used is a multivariate Gaussian,

$$L(\boldsymbol{\kappa}, \boldsymbol{\theta}|\boldsymbol{x}) = \exp\left(-\frac{1}{2}(\boldsymbol{x} - \sigma(\boldsymbol{\kappa}, \boldsymbol{\theta}))^T V^{-1} (\boldsymbol{x} - \sigma(\boldsymbol{\kappa}, \boldsymbol{\theta}))\right) \times \prod_i \text{Gauss}(\theta_i; 0, 1), \tag{4}$$

where $\boldsymbol{x}$ is a vector of all the measurements in each bin, σ is a vector of the parameterized prediction in each bin, and V is the measurements covariance matrix. The θs are the so-called nuisance parameters; they incorporate the systematic uncertainties. The procedure to include the nuisance parameters into the parameterized prediction is by writing each term in the nominal cross section[1], for each bin, as follows,

$$\sigma(\theta) = \sigma_0(1 + \delta\sigma \times \theta), \tag{5}$$

where σ_0 is the nominal prediction, and $\delta\sigma$ is the value of the uncertainty. Systematic uncertainties are due to assumptions and approximations made in theoretical calculations. They include;

- For ggF processes,
  - Numerical integration uncertainty
  - Fixed-order calculation uncertainty
  - Non-perturbative uncertainty
  - Hard resummation phase uncertainty
  - Resumaion uncertainty
  - Matching uncertainty
  - PDF and α_s uncertainties
- For $b\bar{b}H$ and $c\bar{c}H$ processes,
  - QCD scale uncertainty is estimatee by simultaneously varying the renormalisation and the factorisation scales up and down
  - Uncertainties due to the choice of the PDF are estimated by varying m_b and μ_b for $b\bar{b}H$ and by computing the standard deviation of the 100 PDF replicas for the $c\bar{c}H$ process
  - Uncertainties due to the choice of the FxFx merging scale

[1]In principle, one must also parameterize the branching ratio with the nuisance parameters, which was not done in this work. The consequence of this is that, sometimes, we will have more constrained results than we should.

– Statistical uncertainties due to the limited number of simulated events

- For processes that do not depend on κ_c or κ_b,
  - QCD scale variation
  - the choice of Parton Density Functions (PDFs)
  - the choice of the value of α_s
  - parton shower modeling and
  - uncertainties in signal composition

The product of standard Gaussians in Equation (4) are to constraint the values of θ to a standard Gaussian centred at 0 with a standard deviation of 1, instead of letting them vary as free parameters.

Maximizing the likelihood function in Equation (4) yields the best fit values of the parameters of interest (κ). However, it is more convenient, in practice, to minimize the Negative Log-Likelihood (NLL),

$$-2\ln\left(\frac{L(\boldsymbol{\kappa},\hat{\hat{\boldsymbol{\theta}}}(\boldsymbol{\kappa}))}{L(\hat{\boldsymbol{\kappa}},\hat{\boldsymbol{\theta}}(\boldsymbol{\kappa}))}\right) = -2\ln(\Lambda(\boldsymbol{\kappa})), \tag{6}$$

such that this quantity follows a χ^2 distribution in the asymptotic regime (the likelihood is approximately Gaussian). In the numerator the likelihood is maximized by profiling $\boldsymbol{\theta}$ for a set of given values of κ, while the denominator is the maximum unconditional likelihood. Confidence intervals for a certain confidence level (CL) $1-p$ are defined as the values of the NNL that are below the quantile function of the χ^2 distribution, $F^{-1}_{\chi^2_n}(1-p)$. We minimise separately the numerator and denominator in the test statistic in Equation(6). Then, we take the ratio of the minimised likelihoods.

4 Results and discussion

In Figure 3 we see ATLAS measurement plotted with the Standard Model prediction (red line). The blue line is the parameterized cross section with the value of κ_b and κ_c corresponding to the best fit values.

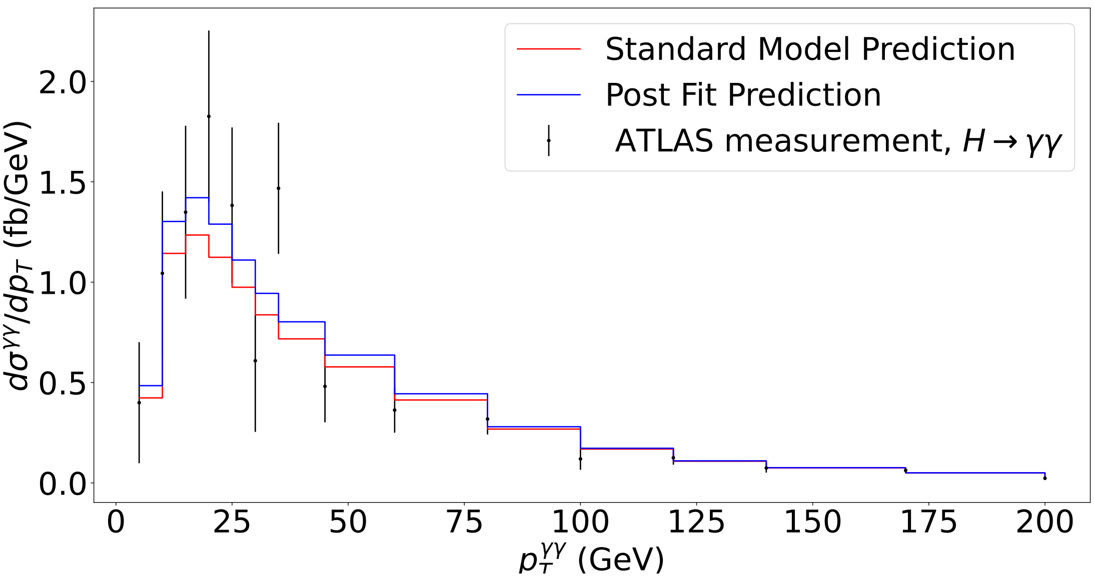

Figure 3: The differential cross-section with respect to p_T as measured by ATLAS (black) for $H \to \gamma\gamma$ final state; the Standard Model cross-section (red), and the post fit prediction of the parameterized cross-section (blue).

To obtain the confidence intervals, and hence the constraints on the value of κ_c at different Confidence Levels (CLs) we plot the NLL with respect to κ_c. Figure 4 shows the NLL scans for κ_c while fixing κ_b to its Standard Model value. The green line corresponds the scan obtained by fitting ATLAS data, while the orange line corresponds to fitting Asimov psudo-data that matches the Standard Model prediction. The reason we are interested in Asimov data is that it gives insight into the systematic uncertainties away from the statistical fluctuations that come with the real data. In addition, it also gives us the expected sensitivity of our analysis design, and the dataset we are using. When optimizing the analysis, we optimize it based on the expected (not observed) sensitivity as the observed sensitivity may fluctuate and we may be biased not to pick the best methods but the methods that pick up the most sensitive fluctuation.

Table 4 shows the confidence intervals for expected and observed κ_c intervals at 68% and 95% CLs. We note that the observed data is more constrained than the expected one; This is because the likelihood function $\sim \kappa_c^2$ leading to two minima in the NLL scan for the observed results, due to the best fit value for κ_c, the two minima merge making the total intervals narrower. However, the results with fixed κ_b are model dependent and a less model-dependant way of fitting the data is by assuming κ_b to be a free parameter as well. Figure 5 shows the NLL scans for κ_c while letting κ_b vary as a free parameter. We note that the results are less constrained than what we had in Figure 4 since the degrees of freedom are now higher. The confidence values obtained are tabulated in Table 4. We note that in all cases, the Standard Model value of the coupling modifier is included.

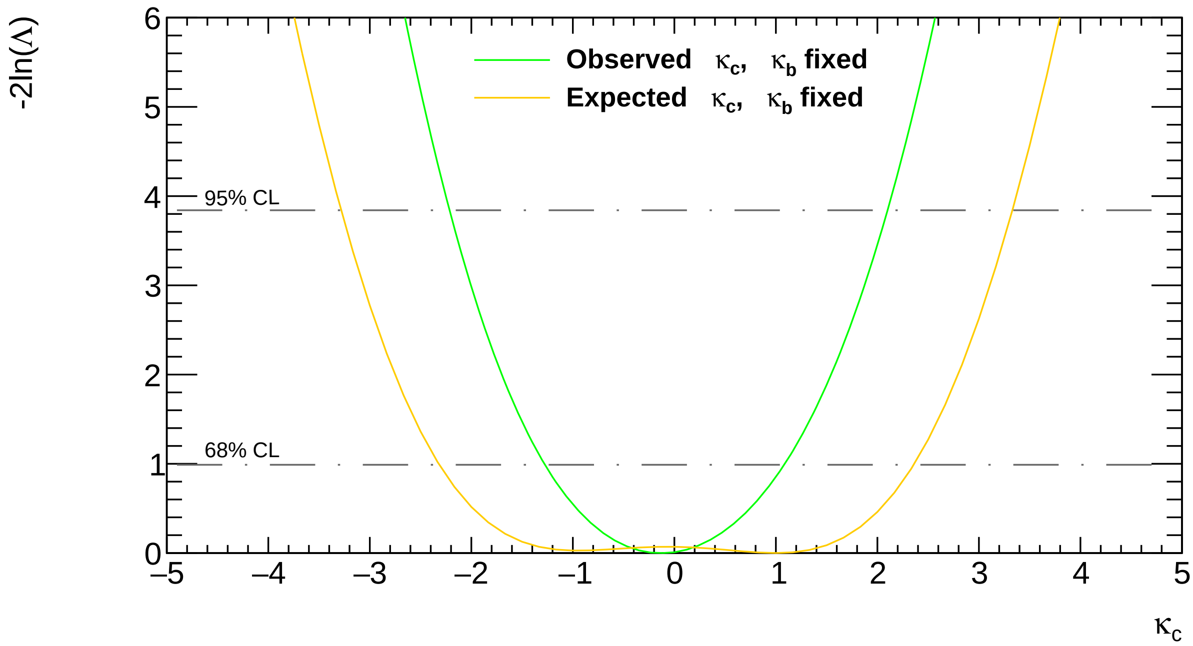

Figure 4: NLL scans for κ_c while fixing κ_b; using ATLAS data (green), and using psudo-data (orange). 95% and 68% CLs are highlighted.

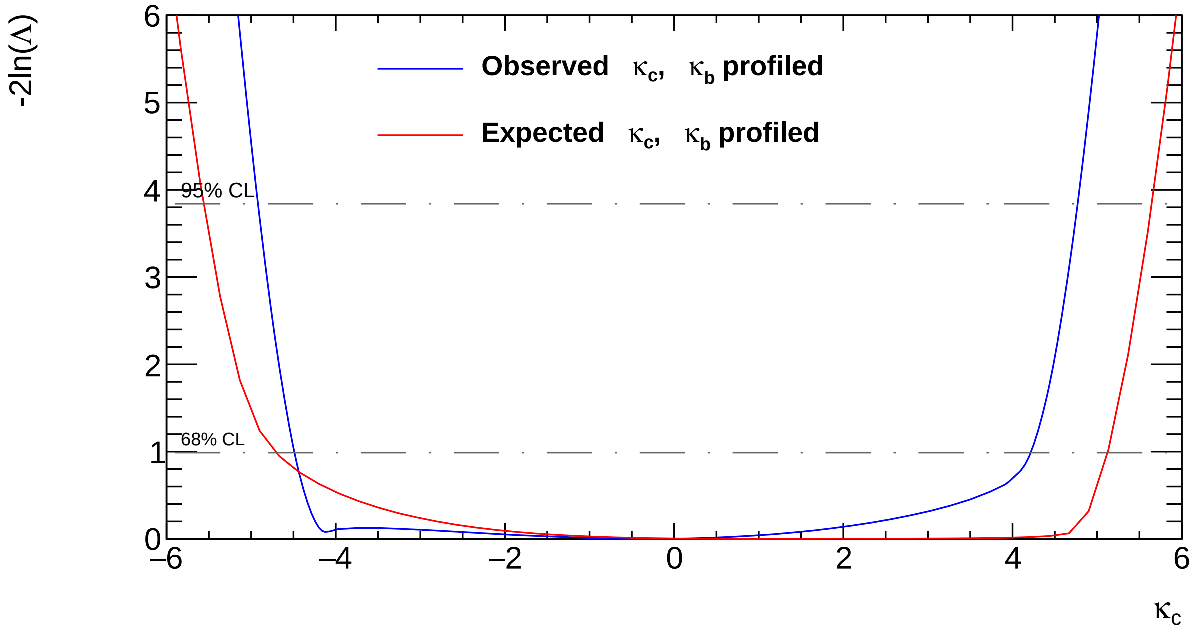

Figure 5: NLL scans for κ_c letting κ_b as a free parameter; using ATLAS data (blue), and using psudo-data (red). 95% and 68% CLs are highlighted.

	68% CL	95% CL
Observed, κ_b profiled	$\kappa_c \in$ [-4.9, 4.2]	$\kappa_c \in$ [-5.3, 4.8]
Expected, κ_b profiled	$\kappa_c \in$ [-5.1, 5.1]	$\kappa_c \in$ [-5.6, 5.6]
Observed, κ_b fixed	$\kappa_c \in$ [-1.3, 1.1]	$\kappa_c \in$ [-2.2, 2.1]
Expected, κ_b fixed	$\kappa_c \in$ [-2.3, 2.4]	$\kappa_c \in$ [-3.3,3.3]

Table 1: 95% and 68% confidence intervals for κ_c observed and expected fits for the case of κ_b fixed and profiled.

To have insights into the effects of systematic uncertainties of the measurements, one can rank the impacts of the nuisance parameters. An impact is defined as follows,

$$\text{impact}_{\kappa_c}^{\pm\sigma}(\theta_i) = \hat{\kappa}_c^{\text{unconditional}} - \hat{\kappa}_c(\theta_i(\pm\sigma)), \tag{7}$$

where σ here is the *standard deviation*. We see from Figure 6, that the parameter with highest impact is due to fixed order $\theta_{\delta\text{FO}}$. We also note that the observed impacts tend to be left sided only, while the expected impacts are always symmetric. This is because the best fit value of κ_c lies at the edge of the confidence interval, both the positive and negative variations of the systematic uncertainty will move the best fit value in the same direrction.

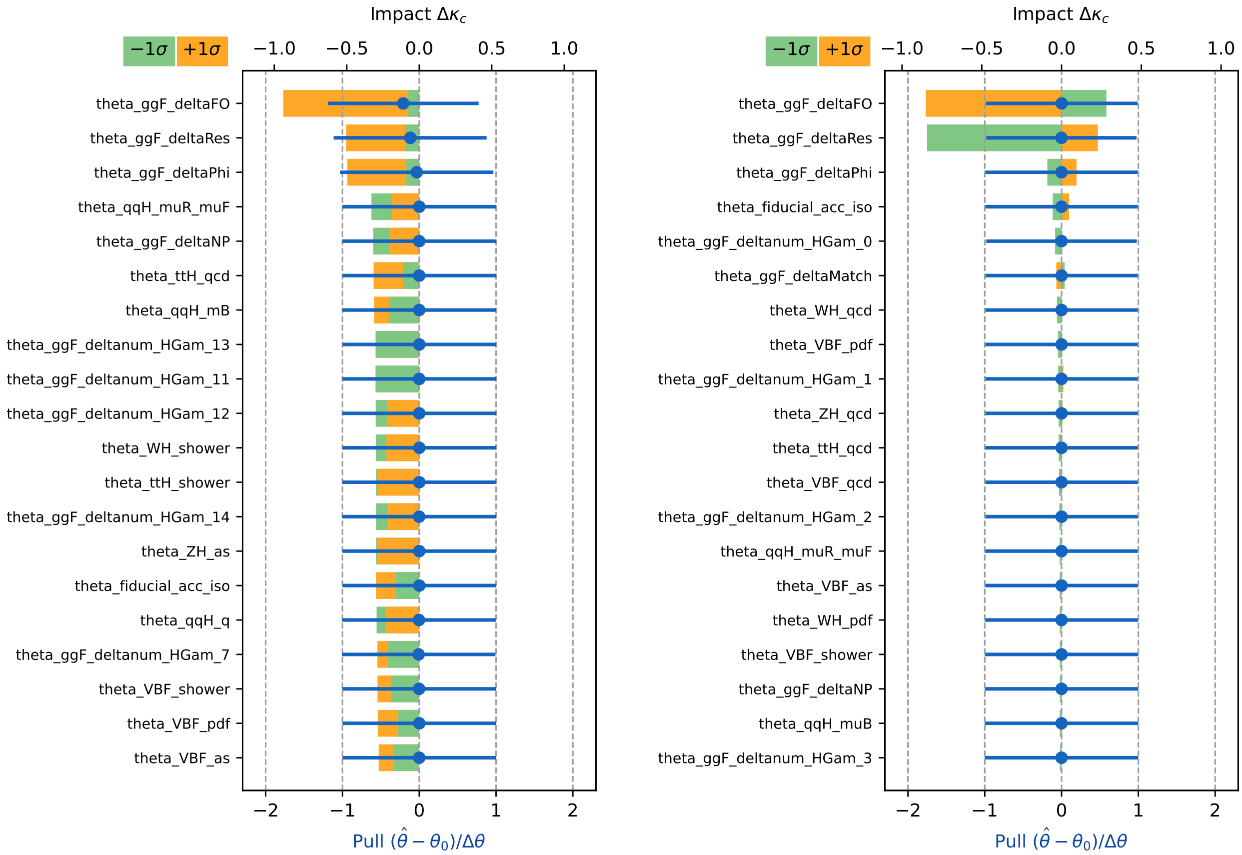

Figure 6: Ranking of the impacts of the nuisance parameters for ATLAS data (left) and Asimov psudo-data (right).

5 Conclusion

The p_T distribution of the Higgs cross section has been analysed to obtain indirect constraints on the coupling modifier κ_c. Maximum likelihood fit was carried out to fit parameterized prediction to ATLAS data. The obtained results are $\kappa_c \in [-5.3, 4.8]$ and $\kappa_c \in [-2.2, 2.1]$ for profiled κ_b and fixed κ_b at 95% CL respectively. The Standard Model value is still included in both confidence intervals.

An insight into the impact of systematic uncertainties on the analysis was obtained by studying Asimov psudo-data that matches the Standard Model prediction, and by ranking the impacts of the nuisance parameters. We observe that the most dominant impact comes from $\theta_{\delta\mathrm{FO}}$. Future prospects for this analysis would be to include the systematic uncertainties into the branching ratio parametrization, and to study the effect of more data on the results.

References

[1] G. Aad et al. "A detailed map of Higgs boson interactions by the ATLAS experiment ten years after the discovery". In: *Nature* 607.7917 (), pp. 52–59. ISSN: 1476-4687. DOI: 10.1038/s41586-022-04893-w. URL: http://dx.doi.org/10.1038/s41586-022-04893-w.

[2] G. Aad et al. "Direct constraint on the Higgs–charm coupling from a search for Higgs boson decays into charm quarks with the ATLAS detector". In: *The European Physical Journal C* 82.8 (Aug. 2022). ISSN: 1434-6052. DOI: 10.1140/epjc/s10052-022-10588-3. URL: http://dx.doi.org/10.1140/epjc/s10052-022-10588-3.

[3] G. Aad et al. "Direct constraint on the Higgs–charm coupling from a search for Higgs boson decays into charm quarks with the ATLAS detector". In: *The European Physical Journal C* 82.8 (). ISSN: 1434-6052. DOI: 10.1140/epjc/s10052-022-10588-3. URL: http://dx.doi.org/10.1140/epjc/s10052-022-10588-3.

[4] G. Aad et al. "Measurement of the total and differential Higgs boson production cross-sections at $\sqrt{s}$=13 TeV with the ATLAS detector by combining the $H \rightarrow ZZ^* \rightarrow 4\ell$ and $H \rightarrow \gamma\gamma$ decay channels". In: *Journal of High Energy Physics* 2023.5 (). ISSN: 1029-8479. DOI: 10.1007/jhep05(2023)028. URL: http://dx.doi.org/10.1007/JHEP05(2023)028.

[5] G. Aad et al. "Observation of a new particle in the search for the Standard Model Higgs boson with the ATLAS detector at the LHC". In: *Physics Letters B* 716.1 (), pp. 1–29. ISSN: 0370-2693. DOI: 10.1016/j.physletb.2012.08.020. URL: http://dx.doi.org/10.1016/j.physletb.2012.08.020.

[6] Riccardo Maria Bianchi and ATLAS Collaboration. "ATLAS experiment schematic or layout illustration". General Photo. 2022. URL: https://cds.cern.ch/record/2837191.

[7] Fady Bishara et al. "Constraining Light-Quark Yukawa Couplings from Higgs Distributions". In: *Physical Review Letters* 118.12 (). ISSN: 1079-7114. DOI: 10.1103/physrevlett.118.121801. URL: http://dx.doi.org/10.1103/PhysRevLett.118.121801.

[8] Petar Bokan et al. *Combination of the total inclusive and differential Higgs boson cross-sections and interpretations*. Tech. rep. Geneva: CERN, 2022. URL: https://cds.cern.ch/record/2804361.

[9] S. Chatrchyan et al. "Observation of a new boson at a mass of 125 GeV with the CMS experiment at the LHC". In: *Physics Letters B* 716.1 (), pp. 30–61. ISSN: 0370-2693. DOI: 10.1016/j.physletb.2012.08.021. URL: http://dx.doi.org/10.1016/j.physletb.2012.08.021.